On the Electrostatics of Bernal-Stacked Few-Layer Graphene on Surface-Passivated Semiconductors

Yasin Khatami, *Student Member, IEEE*, Hong Li, *Member, IEEE*, Wei Liu, *Member, IEEE*, and Kaustav Banerjee, *Fellow, IEEE*

***Abstract*—The superb properties of graphene such as high mobility, broad spectral range of optical transparency, high mechanical flexibility, and impermeability to moisture have made it a promising material for transparent conductor (TC) applications. To optimize the properties of graphene-based TCs, an in-depth understanding of the properties of graphene layers on different materials is crucial. In this paper, the electrostatics and charge screening of Bernal-stacked few-layer graphene (FLG) on surface-passivated semiconductors (SC) are investigated. A self-consistent method is developed, which calculates the equilibrium characteristics of the Schottky barrier at the interface and the charge distribution arising from the impurities on FLG and charge transfer from the SC to FLG. The developed model is applied to FLG/Si structures, and the charge distribution and charge screening effects are investigated. It is shown that with proper selection of doping concentration, the barrier height of the FLG/Si structure under study can be reduced by more than 400 mV, which is crucial in improving the contact resistance between FLG and SC. The self-consistent method and the analysis provide a pathway toward high-performance design of FLG-based TCs.**

***Index Terms*—Electrostatics, few-layer grapheme (FLG), Schottky barrier, surface-passivated semiconductor (SC).**

I. Introduction

With the rapid growth of the market demand for transparent electrodes in touch panels, displays, light emitting devices, light sensors, and solar cells, alternative materials have been studied to replace the widely used indium tin oxide (ITO) due to its high cost, fragility, and limited supply of indium. Graphene has provided new opportunities toward transparent conductor (TC) applications because of its high optical transparency, high carrier mobility, high electrical conductivity, low cost of fabrication, high thermal stability, and high mechanical flexibility [1]–[3]. Graphene is an excellent heat conductor [4], which can be utilized to remove heat efficiently from solar cells and other devices. Moreover, recent demonstration of graphene's outstanding resilience against electrostatic discharge (ESD) has made it an attractive material for ESD protection applications as well as various TC applications that require robustness against ESD for their wide scale deployment [5]. Furthermore, the growth and quality control of large-area and high-quality graphene sheets have been demonstrated experimentally through chemical vapor deposition (CVD) method [6]–[8].

Few-layer graphene (FLG) exhibits higher electrical conductivity (σ) compared to single-layer graphene (SLG) with optical transmittance (T_{op}) of $\sim$90% for three-layer FLG [3]. Graphene layers can have different stacking in graphite. The Bernal (ABA)-stacking is preferred over the other stacking types due to its prevalence in commonly used highly oriented pyrolytic graphite (HOPG) and natural graphite, and is studied in this paper.

The optical and electrical properties of SLG and FLG have been studied to some extent through experimental work [9]–[20]. It has been shown that SLG on hydrogen-passivated Si surface [9] exhibits properties close to the Schottky–Mott limit [21], [22], where no Fermi level pinning is observed allowing Schottky barrier height (Φ_B) adjustment in these structures. This can lead to significantly low contact resistivity between graphene and SC. On the other hand, there is a limited understanding of the properties of FLG on SC especially for solar cell applications. With the new advancements in this field, it is crucial to develop a theoretical model that can capture the physics and predict the properties of FLG on SC.

It has been well established that the electrical conductivity of FLG depends on the carrier concentration and carrier mobility in the FLG layers. The carrier concentration in FLG can be improved by introduction of ionized impurities and charge transfer from the substrate. However, the impurities act as scattering centers for carriers in FLG, which leads to a lower mobility. Therefore, an optimization of the carrier concentration and carrier mobility is required to improve the electrical properties of FLG. The contact resistivity between FLG and SC (which depends on Φ_B) is another important factor in optimization of FLG/SC properties.

In [23]–[32], the electrostatics and charge screening of FLG on oxide has been reported. In [33] and [34], a model is developed for calculation of the bandstructure and charge screening of FLG in presence of an applied electric field. It has been shown

Manuscript received June 13, 2013; revised October 20, 2013; accepted November 18, 2013. Date of publication November 28, 2013; date of current version January 6, 2014. This work was supported by the U.S. Department of Energy sponsored Bay Area Photovoltaic Consortium. The review of this paper was arranged by Associate Editor A. Ghosh.

Y. Khatami was with the Department of Electrical and Computer Engineering, University of California, Santa Barbara, CA 93106 USA. He is now with the Intelligent Memory Solutions Group, SanDisk Corp., Milpitas, CA 95035 USA (e-mail: yasin.khatami@sandisk.com).

H. Li was with the Department of Electrical and Computer Engineering, University of California, Santa Barbara, CA 93106 USA. He is now with the Emerging Memory Group, Micron Technology, Boise, ID 83707 USA (e-mail: hongli@micron.com).

W. Liu and K. Banerjee are with the Department of Electrical and Computer Engineering, University of California, Santa Barbara, CA 93106 USA (e-mail: liuwei@ece.ucsb.edu; kaustav@ece.ucsb.edu).

Color versions of one or more of the figures in this paper are available online at http://ieeexplore.ieee.org.

Digital Object Identifier 10.1109/TNANO.2013.2293355

1536-125X © 2013 IEEE. Personal use is permitted, but republication/redistribution requires IEEE permission.
See http://www.ieee.org/publications_standards/publications/rights/index.html for more information.

that an external electric field modifies the bandstructure of FLG and induces a band overlap or a bandgap. Similar studies on the bandstructure of FLG on different oxides have been reported through self-consistent approaches, such as Thomas–Fermi approximation and minimization of energy [23], [35], [36]. While in these studies, the FLG is assumed to be on an insulating material, the characteristics of FLG on a semiconductor (SC) are not understood well. FLG on SC forms a Schottky barrier similar to a metal–SC junction. Due to the low density of states (DOS) of FLG, its work function varies with the amount of charge transferred to or from the substrate. Therefore, a new model needs to be developed to capture this effect, which can predict the height of Schottky barrier as well. The work function difference between FLG and SC and the resulting electric field leads to a distribution of charge amongst the FLG layers. In [13], a simple model is developed for calculation of the Schottky barrier height for SLG on SC. However, that model cannot be applied to FLG on SC structures due to the charge distribution and charge screening effect of FLG.

In this paper, we investigate the electrostatics of ABA-stacked FLG on surface-passivated SC by developing a self-consistent calculation that takes into account the charge transfer from the substrate and the band filling of FLG. It is assumed that the surface-passivated SC is free of dangling bonds and interface dipoles [9]. We consider both the equilibrium and nonequilibrium situations for the FLG-SC structure. For applications of FLG as TC in solar cells, the voltage drop between the FLG and the SC is small compared to the total voltage of the cell. Therefore, if the charge density variation due to the current flow can be neglected, the electrostatics of the FLG-SC structure is very close to the equilibrium condition. On the other hand, the nonequilibrium situation becomes important in measurement of the Φ_B between FLG and SC. In these measurements, a reverse bias is applied to the structure, and Φ_B is measured by studying the temperature dependence of the reverse current assuming that Φ_B is constant in the process. However, as will be shown here, the Φ_B does not necessarily remain constant when the reverse bias changes. Therefore, the model should be able to capture this effect.

With the developed model we study the barrier height, doping of FLG and interface properties of FLG-Si structures as a function of Si doping, impurity doping of FLG and number of graphene layers (N). The developed model and the results of this paper provide a path toward improving the properties of FLG on SC. The transport problem in FLG is outside of the scope of the current paper and will be studied in future work.

II. FLG on SC Structure

The FLG-SC structure is shown in Fig. 1(a). Each layer is represented by a number, with 1 corresponding to the layer on top and N corresponding to the bottom layer in contact with the SC. The SC has a uniform doping concentration of N_D, and $N_{\rm imp}$ represents the impurity concentration on the top-most graphene layer. The impurities are either added intentionally to control the carrier concentration of FLG or unintentionally introduced during fabrication or through the environment. For simplicity, we only assume the impurities over the top layer.

III. Derivation of Model

The band structure for the FLG on SC is shown in Fig. 1(b) and (c). In equilibrium [see Fig. 1(b)], the Fermi levels on both sides $(E_{\rm FS}$ and $E_{\rm FG})$ line up. The Dirac point of FLG and the electron affinity level of the SC are represented by $E_{\rm Dirac}$ and $e\chi_S$, respectively. We define the relative position of the Fermi level in layer j with respect to the Dirac point of FLG as $\Delta E_{F,j}$, and $e\Phi_n = E_C - E_{\rm FS}$ for n-type SC in the bulk, where e is the unit electron charge. We consider spacing between the FLG and the SC with length d_i and a relative dielectric constant of ε_i and a voltage drop of V_i at the interface. This is consistent with the theoretical and experimental study in [12] of graphene on hydrogenated Si surface. We will study this interface and its effect on the Φ_B after we develop the electrostatic model. We assume that there is no polarization at the interface. Such an interface has been demonstrated experimentally on SLG/Si:H structure [9].

The band diagram for the nonequilibrium case is shown in Fig. 1(c), where the applied voltage $(V_{\rm ap})$ shifts the Fermi levels in SC and FLG with respect to each other. The band diagram of Fig. 1(c) corresponds to a negative voltage on the FLG side compared to the SC. In the nonequilibrium situation, Φ_B, V_i, and $\Delta E_{F,j}$ have different values compared to the equilibrium situation.

The band structure of ABA-FLG is computed using the **k**·**p** Hamiltonian (H) with the in-plane nearest-neighbor coupling of 3.16 eV and interlayer vertical coupling of 0.39 eV [33]. The electrostatic potential is included in the diagonal terms of H. The density matrix is defined as $f_0(H - E_{\rm FG}.I)$, where f_0 is the Fermi-Dirac distribution and I is the identity matrix [37]. The carrier concentration at each layer is calculated by summing up the diagonal elements of the density matrix for all **k**, where **k** is the electron wavevector [32]. The spin and valley degeneracy factors with both equal to 2 are used in calculation of the carrier concentration.

For the structure shown in Fig. 1, the carrier density in FLG changes due to the contribution of the ionized impurities on top of FLG and the charge transferred from SC to FLG. For the case of donor-type impurities and donor doping in SC, a negative charge is induced in FLG as shown in Fig. 1(b). Depending on the amount of charge on each layer, the electrostatic potential would be different for each layer as illustrated in Fig. 1(a). Furthermore, the asymmetric charge distribution leads to an electric field across the layers inducing band overlap in FLG, which is taken into account in the **k**·**p** description of the FLG.

We develop an iterative self-consistent method to calculate the charge distribution in FLG, which is illustrated in Fig. 2. The self-consistent calculation consists of two loops. The inner loop neglects the screening effects in FLG and calculates the charge distribution and barrier height. The screening effect is then introduced through the outer loop. The simulation begins by assuming an initial value for the potential distribution in each layer U_j $(j = 1, 2, \ldots, N)$ and an SC charge (Q_S). The total

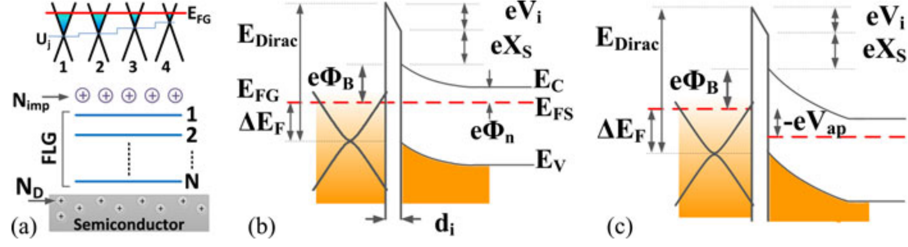

Fig. 1. FLG on semiconductor. (a) Structure of FLG on SC and schematic illustration of the electrostatic potential along the various graphene layers and (b) band structure for FLG on SC under equilibrium. (c) Band structure for FLG on SC under an applied voltage. In (b) and (c), FLG is on the left and the SC is on the right, and $E_{\rm Dirac}$ corresponds to the Dirac point of layer *N,* which is in contact with the SC. Only one of the subbands is shown. The parameters are $E_{\rm FG}$: Fermi level of FLG.; U_j: electrostatic potential at layer j; N_D: doping density of SC; $N_{\rm imp}$: impurity concentration on top of FLG; ΔE_F: relative position of $E_{\rm FG}$ and $E_{\rm Dirac}$; Φ_B: barrier height; χ_S: electron affinity of SC; V_i: voltage drop at the interface; d_i: spacing between FLG and SC; E_C, E_V: conduction and valence bands in SC; $e\Phi_n = E_C - E_{\rm FS}$ is defined in the bulk far from the junction.

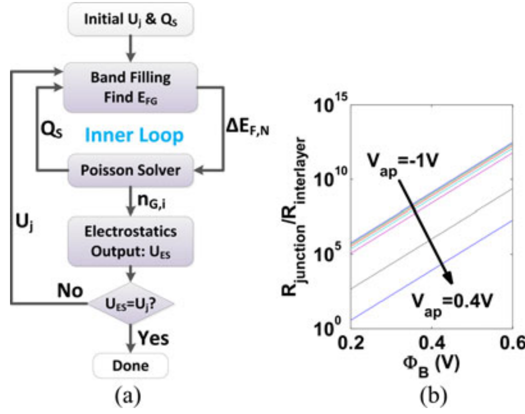

Fig. 2. (a) Self-consistent procedure for calculation of charge distribution in FLG on SC. The inner loop calculates the charge distribution in FLG and the Schottky barrier height by neglecting the screening in FLG. The outer loop takes into account the screening effect in FLG. The texts on the connecting lines indicate the main parameters passed from each step to the next. (b) $R_{\rm junction}/R_{\rm interlayer}$ ratio as a function of Φ_B for $V_{\rm ap} = -1$ V to $+0.4$ V in steps of 0.2 V.

charge per unit area on FLG (n_G) is the sum of the charge transferred from the SC and the impurities, $n_G = -(N_{\rm imp}+Q_S/e)$. The $N_{\rm imp}$ has a positive (negative) value for donor (acceptor) impurities. Given the U_j and n_G, we can compute the band structure of FLG and find the position of the Fermi level in FLG [33]. This step is illustrated as the *Band Filling* block in Fig. 2. Note that as illustrated in Fig. 1(a), $E_{\rm FG}$ is constant across all the layers, but U_j is different, therefore, $\Delta E_{F,j}$ is different for each layer. The calculated $E_{\rm FG}$ determines the Schottky barrier height by inspecting Fig. 1(b) or (c)

$$\Phi_B = \frac{E_{\rm Dirac}}{e} - \frac{\Delta E_{F,N}}{e} - V_i - {\rm X}_S \tag{1}$$

$$V_i = \frac{d_i}{\varepsilon_i \varepsilon_0} Q_S \tag{2}$$

where $\Delta E_{F,N}$ is defined as ΔE_F for the layer N in contact with the SC. With Φ_B calculated from (1), we can calculate a new value for Q_S. In the full depletion approximation regime, the SC charge is calculated from [38]

$$Q_S = \sqrt{2eN_D\varepsilon_S\left(\Phi_B - V_{\rm ap} - \Phi_n - k_BT/e\right)} \tag{3}$$

where ε_S is the dielectric constant of the SC, k_B is the Boltzmann constant, and T is the temperature. Now with the new Q_S, we can calculate a new value for $E_{\rm FG}$. To find the self-consistent solution we iterate on the band filling and Poisson solver procedures until $E_{\rm FG}$ converges. It can be observed from (3) that Q_S depends on $V_{\rm ap}$. Therefore, Φ_B and V_i also depend on $V_{\rm ap}$ through (1) and (2). We also note that the use of depletion approximation is valid when the magnitude of the surface potential in SC ($\Phi_S = -\Phi_B + \Phi_n + V_{\rm ap}$) *is larger than a few* k_BT/e [38] and the density of mobile charge is negligible. If these conditions are not valid, the Poisson equation has to be solved. It can be shown from the results that the depletion approximation is valid for the cases studied here.

Next, we have to consider the screening in the FLG arising from the nonuniform distribution of charges in FLG layers. We consider the FLG as parallel plates with zero thickness that are 0.34 nm apart and have respective electron densities $n_{G,i}$, which are calculated from the density matrix. The electric field between layers j and j+1 is calculated from

$$F_{j,j+1} = \frac{e}{\varepsilon_G\varepsilon_0}\left(N_{\rm imp} + \sum_{i=1}^{j} n_{G,i}\right) \tag{4}$$

where ε_0 is the vacuum permittivity and ε_G is the relative permittivity of the interlayer regions without the screening effect of π-electrons of carbon atoms, and similar to [33] we set ε_G = 2. From (4), we calculate a new set of potential $U_{\rm ES}$ and compare it to U_j. This step is shown by the block *Electrostatics* in Fig. 2. By substituting the $U_{\rm ES}$ into U_j, a new value for $E_{\rm FG}$ can be calculated through the outmost loop in Fig. 2. The procedure continues until the $U_{\rm ES}$ and U_j converge. We developed the simulation code according to the procedure described as follows. The code is written for parallel processing, and the simulation takes about 1 to 5 min to converge for each bias point on six cores (2.5 GHz). Depending on the number of graphene layers and the simulation setup, the inner loop converges in 5–8 iterations, and the outer loop converges in less than 20 iterations. The convergence and speed can be tuned by using a linear under-relaxation algorithm of $U_{j,\rm new} = \alpha U_{\rm ES} + (1-\alpha)U_{j,\rm old}$ with $\alpha = 0.1$ to 0.2 leading to fast convergence.

In this paper, the applied voltage is assumed to drop entirely on the FLG/SC junction. Therefore, the series resistance of the SC and the voltage drop on the graphene

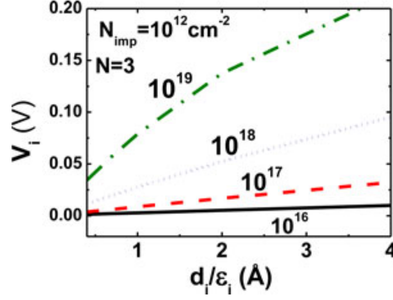

Fig. 3. Variation of the voltage drop at the interface as a function of d_i/ε_i for different SC doping levels in a FLG/Si:H structure. FLG has three layers, and the concentration of impurities is 10^{12} cm^{-2}. The SC doping is shown on each curve in cm^{-3}. For low values of SC doping, V_i is negligible. V_i becomes significant compared to the barrier height and ΔE_F as SC doping increases.

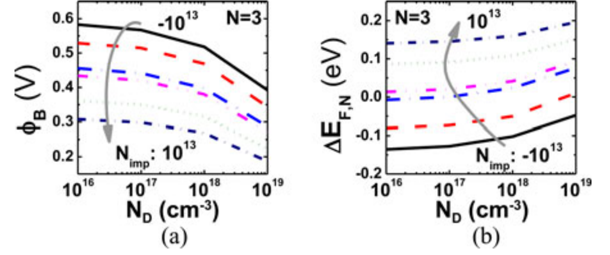

Fig. 4. Properties of trilayer FLG on Si:H structure. (a) Barrier heights and (b) relative positions of Fermi level in layer N in contact with the SC versus Si doping for different values of $N_{\rm imp}$. The values of $N_{\rm imp}$ are -10^{13}, -5×10^{12}, -5×10^{11}, 5×10^{11}, 5×10^{12}, and 10^{13} cm^{-2} from top to bottom curves in (a) and from bottom to top curves in (b). A value of $N_{\rm imp} < 0$ indicates acceptor-type impurity concentration, and $N_{\rm imp} > 0$ indicates donor-type impurity concentration. SC dopants are donors. A positive (negative) value of ΔE_F indicates electron (hole) accumulation in the FLG.

layers is set to zero. Such an assumption is valid provided that the FLG/SC junction resistance ($R_{\rm junction}{=}V_{\rm ap}/I$) is much higher than the interlayer resistance between graphene layers ($R_{\rm interlayer}$). The thermionic emission current is calculated from $J = AA{*}T^2\exp(-e\Phi_B/k_BT)[\exp(eV_{\rm ap}/nk_BT) - 1]$ [38], where A is the area and $A*$ is the Richardson constant and is set to 252 cm$^{-2}\cdot$K^{-2} [9]. The plot of $R_{\rm junction}/R_{\rm interlayer}$ is shown in Fig. 2(b) as a function of the Schottky barrier height and for different values of $V_{\rm ap}$ with $R_{\rm interlayer} = \rho_I t/A$. The ρ_I is the c-axis interlayer resistivity of FLG and is set to 5×10^{-5} $\Omega\cdot$m [39], and $t = 0.35$ nm is the interlayer spacing of FLG. It can be observed from Fig. 2(b) that the $R_{\rm junction}/R_{\rm interlayer}$ is much larger than 1 for $V_{\rm ap} < 0$. Therefore, the assumption of voltage drop only at the FLG/SC interface is valid for reverse bias. For $V_{\rm ap} > 0$ and for small values of Φ_B, this assumption may not be valid. Our analysis here is based on the reverse bias regime.

Furthermore, we assume that the metal to FLG contact is far enough from the interface so that we can ignore the current crowding effects. This is a valid assumption since the current crowding in metal-FLG contact is generally happening under the contact area, and due to the relatively low values of ρ_I, the current spreads out rapidly through FLG layers [40], [41].

IV. Results and Discussion

Next, we apply the developed procedure to FLG on hydrogen-passivated silicon (Si:H) surface with an applied voltage of 10 mV under the depletion approximation, and discuss the effects of different parameters on the properties of the FLG and barrier height. We assume a value of 4.5 eV for the $E_{\rm Dirac}$ of FLG and a value of 4.05 eV for Si electron affinity level.

First, we consider the effect of the spacing between the FLG and Si. Fig. 3 shows the voltage drop at the interface (V_i) as a function of the interface effective distance, d_i/ε_i, for different values of substrate doping for a sample FLG/Si:H structure. In [12], the spacing between graphene and Si (hydrogenated surface) is reported to be $\sim$4 Å. Earlier studies on Si:H interface have considered a value of 4 for the relative dielectric constant of the interface [42]–[44]. From Fig. 3, it can be observed that the variation of V_i [which is a linear function of Q_S (see 2)] is negligible when the substrate doping is less than 10^{17} cm^{-3}. For larger values of N_D, the variation of V_i becomes important as d_i/ε_i is varied. The reason is that for low values of SC doping, the amount of charge transferred from the SC to FLG is small, and the voltage drop at the interface is negligible. However, for higher SC doping, the amount of charge transferred from SC to FLG is high enough to create a relatively large V_i. From the experimental results of Yang *et al.* [4] (with $N_D{\sim}10^{17}$ cm^{-3}) we can determine a value of V_i $\sim$0.01 to 0.02 V, which corresponds to a $d_i/\varepsilon_i{\sim}$4/4 Å $= 1$ Å consistent with earlier work [12], [42]–[44], and will be considered for the rest of the results presented hereafter.

The calculated barrier heights and the relative positions of the Fermi level for layer N ($\Delta E_{F,N}$) for typical FLG/Si:H structures with $N = 3$ are shown in Fig. 4. The SC dopants are assumed to be donors, and the impurity doping is varied between donor and acceptor types. The values of the $N_{\rm imp}$ are within experimental limits, and are chosen such that the $E_{\rm FG}$ can be varied by a few 100 meV. It can be observed that an increase in SC doping level leads to a smaller barrier height. This is attributed to the higher charge transferred from SC to FLG (Q_S) with increasing N_D, which increases the charge concentration in FLG and increases $\Delta E_{F,N}$. According to (1), an increase of $\Delta E_{F,N}$ leads to a lower value of Φ_B and vice versa. (Note that V_i varies with Q_S, but the major contribution is due to the variation of ΔE_F.) Therefore, Φ_B reduces as N_D increases. For donor-type impurities ($N_{\rm imp} > 0$), an increase of $N_{\rm imp}$ leads to a higher electron concentration in FLG, and higher $\Delta E_{F,N}$, which leads to lower Φ_B as observed in Fig. 4(a).

For acceptor-type impurities ($N_{\rm imp} > 0$), an increase of the doping concentration (more negative values of $N_{\rm imp}$), leads to a lower electron concentration in FLG, and lower $\Delta E_{F,N}$, which leads to higher Φ_B. It can be observed that for the case studied, the barrier height can be tuned between 200 and 600 mV.

The screening effect in FLG can be observed from Fig. 5, where we have plotted the charge concentration in each layer of FLG with $N = 3$ and $N = 6$ for different values of N_D. It can be observed that the charge density of the bottom layers closer to the SC is under strong control of the SC doping, while the charge density of the top layers is controlled by the impurity concentration. For $N = 6$, the middle layers have low charge

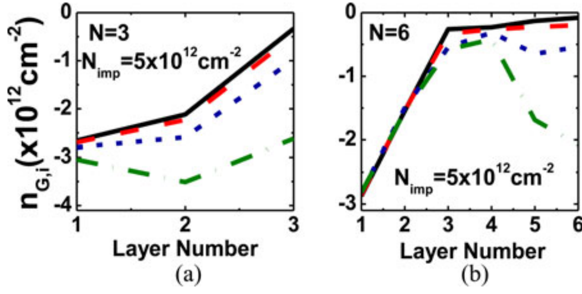

Fig. 5. Charge distribution in the layers of FLG on Si:H for (a) $N = 3$ and (b) $N = 6$ as a function of SC doping. A negative value of $n_{G,i}$ indicates an electron accumulation in layer i. SC doping level N_D is 10^{16}, 10^{17}, 10^{18}, and 10^{19} cm^{-3} from top to bottom. The stronger charge screening of FLG with $N = 6$ can be observed from the dependence of the charge concentration in layer 1 on N_D. The layer with the highest number is in contact with the SC.

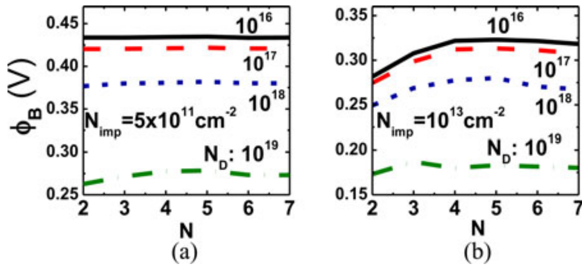

Fig. 6. Barrier height as a function of the number of layers for different values of SC doping and impurity concentrations of (a) 5×10^{11} cm^{-2} and (b) 10^{13} cm^{-2}. SC doping level N_D is reported on each curve in units of cm^{-3}. The increase of Φ_B with N is due to the screening of impurity charges increasing with N. The impurity charges in (a) are screened by a smaller number of layers compared to (b).

density, because the FLG layers effectively screen the impurity and substrate charges. However, for $N = 3$, the screening is not strong enough, leading to a higher charge density in the middle layer.

The effect of the number of layers on the properties of the Schottky barrier formed between the FLG and Si:H also depends on the magnitude of the impurity concentration and SC doping concentration. For a high value of the impurity concentration, more layers are required to screen the impurity charges. We have shown this effect in Fig. 6, where the barrier height is plotted as a function of N for different values of N_D and two values of $N_{\rm imp}$. It can be observed that for constant values of $N_{\rm imp}$ and N_D, the barrier height is a weak function of the number of layers. The reason is that, the charge density in the bottom layer is strongly controlled by the SC doping, and the variation of ΔE_F for the same charge density is small for different values of N. It can also be observed from Fig. 6 that, the variation of Φ_B as a function of N is larger for higher $N_{\rm imp}$ in Fig. 6(b) compared to lower $N_{\rm imp}$ in Fig. 6(a). In this case, the higher value of $N_{\rm imp}$ leads to a higher charge density in the bottom layers, and subsequently lower Φ_B. In Fig. 6(b), this effect is prominent for low values of N where the screening is not strong enough consistent with our earlier discussion.

The effect of a reverse applied bias on the barrier height is shown in Fig. 7 for an FLG/SC structure with $N = 3$ for different values of N_D and $N_{\rm imp}$. It can be observed that Φ_B

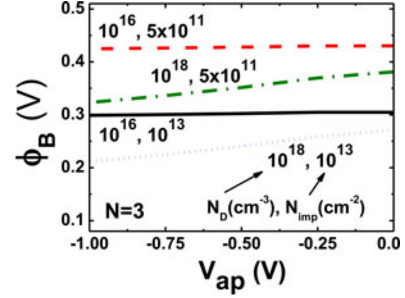

Fig. 7. Barrier height as a function of the applied reverse bias for different values of SC doping and impurity concentrations for $N = 3$. The values of N_D and $N_{\rm imp}$ is reported on each curve. Barrier height exhibits weak dependence on $V_{\rm ap}$.

is a weak function of $V_{\rm ap}$. For $N_D = 10^{16}$ cm^{-3}, the Φ_B is almost independent of $V_{\rm ap}$, while for $N_D = 10^{18}$ cm^{-3}, the Φ_B exhibits a larger variation with respect to $V_{\rm ap}$. This is due to the higher charge transfer from SC to FLG in the case of high N_D, which can be observed from (3).

A large variation of the Schottky barrier height, ideality factor, and Fermi level pinning has been reported in experimental investigations [9]–[20], [45]–[53], which indicates the possibility of tuning the barrier in many different ways. Some examples of the measured barrier heights reported in literature include 0.48 eV in [50], 0.67–1.06 eV in [51], 0.45 eV in [11], 0.25–0.45 eV in [9], and 0.73–0.92 eV in [13]. In [9], a hydrogen-passivated Si surface is in contact with graphene, and our simulations match accurately with the reported barrier heights. In the rest of the measured results, the quality of the interface is not clear. The measured Φ_B values show significant difference between the current–voltage (*J*–*V*) and capacitance–voltage (*C*–*V*) measurements [13], [51]. This discrepancy can be attributed to voltage drop at the interface, series resistance and interface inhomogeneities [54]. Our analysis of the results published in [13], [51] indicate that an interface voltage drop (V_i) due to charge transfer between SC and graphene cannot explain this discrepancy due to the low doping of the SC. That leaves the interface inhomogeneities and the dipoles at the nonideal surface as the source of the difference observed in *J*–*V* and *C*–*V* measurements. Further information such as Hall measurement of the carrier density in graphene (which produces an accurate value for graphene's work function) and/or frequency dependent *C*–*V* measurements can help shine light on the exact nature of the observed discrepancies.

V. Conclusion

In conclusion, we have developed a self-consistent method to calculate the Schottky barrier height and FLG doping for FLG on any surface-passivated SC. The self-consistent method takes into account the screening effects in FLG as well as the interface properties of the FLG/SC structure. The interface parameters can be tuned to reflect the properties of different interfaces. We have applied the developed method to FLG on hydrogen-passivated Si structures, and have studied the characteristics of these structures as a function of the impurity concentration, Si

doping and the number of layers. We have shown that it is possible to tune the interface properties as well as the FLG doping concentration, and reduce the barrier height by few tenths of a volt. The presented results provide important insight into the engineering of FLG for highly efficient TC applications. Although the results are discussed only for ABA (Bernal)-stacked FLG, the developed method can be successfully applied to other types of FLG stacking by including the proper Hamiltonian.

References

[1] A. K. Geim, "Graphene: Status and prospects," *Science (80 −.).*, vol. 324, no. 5934, pp. 1530–1534, 2009.

[2] U. Stoberl, U. Wurstbauer, W. Wegscheider, D. Weiss, J. Eroms, and U. Stöberl, "Morphology and flexibility of graphene and few-layer graphene on various substrates," *Appl. Phys. Lett.*, vol. 93, no. 5, pp. 51903–51906, 2008.

[3] Y. Khatami, W. Liu, J. Kang, and K. Banerjee, "Prospects of graphene electrodes in photovoltaics," in *Proc. SPIE Next Generation (Nano) Photonic Cell Technol. Solar Energy Convers. IV*, 2013, vol. 8824, pp. 88240 T 1–88240 T 6.

[4] A. A. Balandin, "Thermal properties of graphene and nanostructured carbon materials," *Nat. Mater.*, vol. 10, no. 8, pp. 569–581, 2011.

[5] H. Li, C. C. Russ, W. Liu, D. Johnsson, H. Gossner, and K. Banerjee, "ESD characterization of atomically-thin graphene," in *Proc. 34th Electr. Overstress /Electrostatic Discharge Symp. (EOS /ESD)*, 2012, pp. 1–8.

[6] S. Bae, H. R. Kim, Y. Lee, X. Xu, J.-S. Park, Y. Zheng, J. Balakrishnan, T. Lei, Y. Il Song, Y.-J. Kim, K. S. Kim, B. Ozyilmaz, J.-H. Ahn, B. H. Hong, and S. Iijima, "Roll-to-roll production of 30-inch graphene films for transparent electrodes," *Nat. Nanotechnol.*, vol. 5, no. 8, pp. 574–578, 2010.

[7] C. M. Nolen, G. Denina, D. Teweldebrhan, B. Bhanu, and A. A. Balandin, "High-throughput large-area automated identification and quality control of graphene and few-layer graphene films," *ACS Nano*, vol. 5, no. 2, pp. 914–922, 2011.

[8] W. Liu, H. Li, C. Xu, Y. Khatami, and K. Banerjee, "Synthesis of high-quality monolayer and bilayer graphene on copper using chemical vapor deposition," *Carbon*, vol. 49, no. 13, pp. 4122–4130, 2011.

[9] H. Yang, J. Heo, S. Park, H. J. Song, D. H. Seo, K. E. Byun, P. Kim, I. Yoo, H. J. Chung, and K. Kim, "Graphene barristor, a triode device with a gate-controlled Schottky barrier," *Science (80 −.).*, vol. 1140, no. 6085, pp. 1140–1143, 2012.

[10] X. Li, H. Zhu, K. Wang, A. Cao, J. Wei, C. Li, Y. Jia, Z. Li, X. Li, and D. Wu, "Graphene-on-silicon Schottky junction solar cells," *Adv. Mater.*, vol. 22, no. 25, pp. 2743–2748, 2010.

[11] C.-C. Chen, M. Aykol, C.-C. Chang, A. F. J. Levi, and S. B. Cronin, "Graphene–silicon Schottky diodes," *Nano Lett.*, vol. 11, no. 5, pp. 1863–1867, 2011.

[12] Y. Xu, K. T. He, S. W. Schmucker, Z. Guo, J. C. Koepke, J. D. Wood, J. W. Lyding, and N. R. Aluru, "Inducing electronic changes in graphene through silicon (100) substrate modification," *Nano Lett.*, vol. 11, no. 7, pp. 2735–2742, 2011.

[13] S. Tongay, M. Lemaitre, X. Miao, B. Gila, B. R. Appleton, and A. F. Hebard, "Rectification at graphene-semiconductor interfaces: Zero-gap semiconductor based diodes," *Phys. Rev. X*, vol. 2, no. 1, pp. 011002-1–011002-10, 2011.

[14] H. Park, J. A. Rowehl, K. K. Kim, V. Bulovic, and J. Kong, "Doped graphene electrodes for organic solar cells," *Nanotechnology*, vol. 21, no. 50, pp. 505204-1–505204-6, 2010.

[15] T. Feng, D. Xie, Y. Lin, Y. Zang, T. Ren, R. Song, H. Zhao, H. Tian, X. Li, H. Zhu, and L. Liu, "Graphene based Schottky junction solar cells on patterned silicon-pillar-array substrate," *Appl. Phys. Lett.*, vol. 99, no. 23, pp. 233505-1–233505-3, 2011.

[16] J.-P. Shim, M. Choe, S.-R. Jeon, D. Seo, T. Lee, and D.-S. Lee, "InGaN-Based p–i–n solar cells with graphene electrodes," *Appl. Phys. Exp.*, vol. 4, no. 5, pp. 052302-1–052302-3, 2011.

[17] J. Wu, H. A. Becerril, Z. Bao, Z. Liu, Y. Chen, and P. Peumans, "Organic solar cells with solution-processed graphene transparent electrodes," *Appl. Phys. Lett.*, vol. 92, no. 26, pp. 263302-1–263302-3, 2008.

[18] M. Burkhardt, W. Liu, C. G. Shuttle, K. Banerjee, and M. L. Chabinyc, "Top illuminated inverted organic ultraviolet photosensors with single layer graphene electrodes," *Appl. Phys. Lett.*, vol. 101, no. 3, pp. 33302–33304, Jul. 2012.

[19] X. Wang, L. Zhi, and K. Müllen, "Transparent, conductive graphene electrodes for dye-sensitized solar cells," *Nano Lett.*, vol. 8, no. 1, pp. 323–327, 2008.

[20] S. Tongay, T. Schumann, X. Miao, B. R. Appleton, and A. F. Hebard, "Tuning Schottky diodes at the many-layer-graphene/semiconductor interface by doping," *Carbon*, vol. 49, no. 6, pp. 2033–2038, 2011.

[21] W. Schottky, "Zur halbleitertheorie der sperrschicht-und spitzengleichrichter," *Zeitschrift für Phys.*, vol. 113, no. 5–6, pp. 367–414, 1939.

[22] N. F. Mott, "The theory of crystal rectifiers," *Proc. R. Soc. Lond. Ser. A. Math. Phys. Sci.*, vol. 171, no. 944, pp. 27–38, 1939.

[23] F. Guinea, "Charge distribution and screening in layered graphene systems," *Phys. Rev. B*, vol. 75, no. 23, pp. 235433-1–235433-7, 2007.

[24] F. Zhang, B. Sahu, H. Min, and A. H. MacDonald, "Band structure of ABC-stacked graphene trilayers," *Phys. Rev. B*, vol. 82, no. 3, pp. 035409-1–035409-10, 2010.

[25] C. H. Lui, Z. Li, K. F. Mak, E. Cappelluti, and T. F. Heinz, "Observation of an electrically tunable band gap in trilayer graphene," *Nat. Phys.*, vol. 7, no. 12, pp. 944–947, 2011.

[26] S. S. Datta, D. R. Strachan, E. J. Mele, and A. T. C. Johnson, "Surface potentials and layer charge distributions in few-layer graphene films," *Nano Lett.*, vol. 9, no. 1, pp. 7–11, 2008.

[27] S. Latil and L. Henrard, "Charge carriers in few-layer graphene films," *Phys. Rev. Lett.*, vol. 97, no. 3, pp. 036803-1–036803-4, 2006.

[28] J. Nilsson, A. H. C. Neto, F. Guinea, and N. M. R. Peres, "Electronic properties of bilayer and multilayer graphene," *Phys. Rev. B*, vol. 78, no. 4, pp. 045405-1–045405-34, 2008.

[29] F. Guinea, A. H. C. Neto, and N. M. R. Peres, "Electronic states and Landau levels in graphene stacks," *Phys. Rev. B*, vol. 73, no. 24, pp. 245426-1–245426-8, 2006.

[30] S. Russo, M. F. Craciun, T. Khodkov, M. Koshino, M. Yamamoto, and S. Tarucha, "Electronic transport properties of few-layer graphene materials," arXiv Prepr. arXiv1105.1479, 2011.

[31] C. L. Lu, C.-P. Chang, Y.-C. Huang, R.-B. Chen, and M. L. Lin, "Influence of an electric field on the optical properties of few-layer graphene with AB stacking," *Phys. Rev. B*, vol. 73, no. 14, pp. 144427-1–144427-7, 2006.

[32] A. Grüneis, C. Attaccalite, L. Wirtz, H. Shiozawa, R. Saito, T. Pichler, and A. Rubio, "Tight-binding description of the quasiparticle dispersion of graphite and few-layer graphene," *Phys. Rev. B*, vol. 78, no. 20, pp. 205425-1–205425-16, 2008.

[33] M. Koshino, "Interlayer screening effect in graphene multilayers with ABA and ABC stacking," *Phys. Rev. B*, vol. 81, no. 12, pp. 125304-1–125304-7, Mar. 2010.

[34] M. Koshino and T. Ando, "Orbital diamagnetism in multilayer graphenes: Systematic study with the effective mass approximation," *Phys. Rev. B*, vol. 76, no. 8, pp. 085425-1–085425-11, 2007.

[35] Y. Sui and J. Appenzeller, "Screening and interlayer coupling in multilayer graphene field-effect transistors," *Nano Lett.*, vol. 9, no. 8, pp. 2973–2977, 2009.

[36] M. A. Kuroda, J. Tersoff, and G. J. Martyna, "Nonlinear screening in multilayer graphene systems," *Phys. Rev. Lett.*, vol. 106, no. 11, pp. 116804-1–116804-4, 2011.

[37] S. Datta, *Quantum Transport: Atom to Transistor*. Cambridge, U.K.: Cambridge University Press, 2005, p. 419.

[38] S. M. Sze and K. K. Ng, *Physics of Semiconductor Devices*. New York, NY, USA: Wiley-Interscience, 2006.

[39] D. Z. Tsang and M. S. Dresselhaus, "The c-axis electrical conductivity of kish graphite," *Carbon*, vol. 14, no. 1, pp. 43–46, 1976.

[40] Y. Khatami, H. Li, C. Xu, and K. Banerjee, "Metal-to-multilayer-graphene contact—Part I: Contact resistance modeling," *IEEE Trans. Electron. Devices*, vol. 59, no. 9, pp. 2444–2452, Sep. 2012.

[41] Y. Khatami, H. Li, C. Xu, and K. Banerjee, "Metal-to-multilayer-graphene contact—Part II: Analysis of contact resistance," *IEEE Trans. Electron Devices*, vol. 59, no. 9, pp. 2453–2460, Aug. 2012.

[42] W. Mönch, "Barrier heights of real Schottky contacts explained by metal-induced gap states and lateral inhomogeneities," *J. Vac. Sci. Technol. B*, vol. 17, no. 4, pp. 1867–1876, 1999.

[43] T. U. Kampen and W. Mönch, "Lead contacts on Si(111):H-1 $\times$ 1 surfaces," *Surf. Sci.*, vol. 331–333, pp. 490–495, Jul. 1995.

[44] R. Ludeke, G. Jezequel, and A. Taleb-Ibrahimi, "Delocalization effects at metal-semiconductor interfaces," *Phys. Rev. Lett.*, vol. 61, no. 5, pp. 601–604, Aug. 1988.

[45] S. Tongay, T. Schumann, and A. F. Hebard, "Graphite based Schottky diodes formed on Si, GaAs, and 4 H-SiC substrates," *Appl. Phys. Lett.*, vol. 95, no. 22, pp. 222103-1–222103-3, 2009.

[46] H. Zhong, Z. Liu, G. Xu, Y. Fan, J. Wang, X. Zhang, L. Liu, K. Xu, and H. Yang, "Self-adaptive electronic contact between graphene and semiconductors," *Appl. Phys. Lett.*, vol. 100, no. 12, pp. 122108-1–122108-4, 2012.

[47] M. G. Lemaitre, E. P. Donoghue, M. A. McCarthy, B. Liu, S. Tongay, B. Gila, P. Kumar, R. K. Singh, B. R. Appleton, and A. G. Rinzler, "Improved transfer of graphene for gated Schottky-junction, vertical, organic, field-effect transistors," *ACS Nano*, vol. 6, no. 10, pp. 9095–9102, 2012.

[48] M. Mohammed, Z. Li, J. Cui, and T. Chen, "Junction investigation of graphene/silicon Schottky diodes," *Nanoscale Res. Lett.*, vol. 7, no. 1, pp. 1–6, 2012.

[49] S. Sonde, F. Giannazzo, V. Raineri, R. Yakimova, J.-R. Huntzinger, A. Tiberj, and J. Camassel, "Electrical properties of the graphene/4 H-SiC (0001) interface probed by scanning current spectroscopy," *Phys. Rev. B*, vol. 80, no. 24, pp. 241406-1–241406-4, 2009.

[50] Y. An, A. Behnam, E. Pop, and A. Ural, "Metal-semiconductor-metal photodetectors based on graphene/p-type silicon Schottky junctions," *Appl. Phys. Lett.*, vol. 102, no. 1, pp. 013110-1–013110-5, 2013.

[51] S. Shivaraman, L. H. Herman, F. Rana, J. Park, and M. G. Spencer, "Schottky barrier inhomogeneities at the interface of few layer epitaxial graphene and silicon carbide," *Appl. Phys. Lett.*, vol. 100, no. 18, pp. 183112-1–183112-4, 2012.

[52] S. A. Reshanov, K. V Emtsev, F. Speck, K. Gao, T. K. Seyller, G. Pensl, and L. Ley, "Effect of an intermediate graphite layer on the electronic properties of metal/SiC contacts," *Phys. Status Solidi*, vol. 245, no. 7, pp. 1369–1377, 2008.

[53] X. Miao, S. Tongay, M. K. Petterson, K. Berke, A. G. Rinzler, B. R. Appleton, and A. F. Hebard, "High efficiency graphene solar cells by chemical doping," *Nano Lett.*, vol. 12, no. 6, pp. 2745–2750, 2012.

[54] R. T. Tung, "Recent advances in Schottky barrier concepts," *Mater. Sci. Eng. R Rep.*, vol. 35, no. 1, pp. 1–138, 2001.

Yasin Khatami (S'05) received the Ph.D. degree in electrical and computer engineering from the University of California, Santa Barbara, USA, in 2013.

He is currently a Senior Device Engineer at SanDisk Corporation, Milpitas, CA, USA. His current research interests include the exploration of emerging nano-transistors for near and long-term future integration in energy-efficient integrated circuits, carbon electronics, and Flash memory.

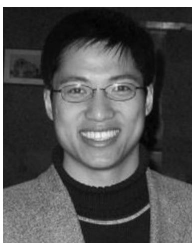

Hong Li (S'07–M'12) received the Ph.D. degree in electrical and computer engineering from the University of California, Santa Barbara, USA, in 2012.

He is currently an Emerging Memory Engineer with Micron Technology, Inc., Boise, ID, USA. He has authored or coauthored more than 30 publications.

Dr. Li is the recipient of the Best Paper Award and the Best Student Paper Award of the 34th EOS/ESD Symposium in 2012.

Wei Liu (M'10) received the Ph.D. degree in chemistry from the Institute of Chemistry, Chinese Academy of Sciences, Beijing, China, in 2008.

From 2008 to 2010, he was a Postdoctoral Fellow with the Department of Material Science and Engineering, University of California, Los Angeles, USA, where he is currently a Postdoctoral Fellow in the Department of Electrical and Computer Engineering. He has authored or coauthored more than 50 refereed journal, conference, and workshop publications. His current research interests include the synthesis of low-dimensional materials (carbon nanotube, graphene, and transition-metal dichalcogenides) as well as the exploration of low-dimensional materials based novel devices.

Dr. Liu is the recipient of the Best Paper Award and the Best Student Paper Award of the 34th EOS/ESD Symposium in 2012.

Kaustav Banerjee (S'92–M'99–SM'03–F'12) received the Ph.D. degree in electrical engineering and computer sciences from the University of California, Berkeley, USA, in 1999.

In 2002, he joined as a Faculty Member with the Department of Electrical and Computer Engineering, University of California, Santa Barbara (UCSB), where he has been a Full Professor since 2007. Prior to joining UCSB, he was a Research Associate with the Center for Integrated Systems, Stanford University, Stanford, CA, from 1999 to 2001. His research interests include nanometer-scale issues in CMOS VLSI as well as emerging nanoelectronics. He is currently involved in exploring the physics, technology, and applications of low-dimensional nanomaterials for the next-generation green electronics, photonics, and bioelectronics.

Dr. Banerjee's ideas and innovations chronicled in over 275 papers have not only received thousands of citations (with h-index of 47) but also have played a decisive role in steering worldwide research and development efforts. He is one of five engineers worldwide to receive the Friedrich Wilhelm Bessel Research Award from the Alexander von Humboldt Foundation, Germany, in 2011, for his outstanding contributions in nanoelectronics. He is also the recipient of a JSPS Invitation Fellowship from the Japan Society for the Promotion of Science for 2013–14. His technical contributions have been recognized with numerous other awards and honors including an IBM Faculty Award in 2008, an IEEE Micro Top Picks Award in 2006, the ACM-SIGDA Outstanding New Faculty Award in 2004, and Best Paper Awards at the ACM/IEEE Design Automation Conference in 2001 and the EOS/ESD Symposium in 2012. He has been serving as a Distinguished Lecturer of the IEEE Electron Devices Society since 2008.